Construction and Building Materials 511 (2026) 145232

Contents lists available at ScienceDirect

Construction and Building Materials

journal homepage: www.elsevier.com/locate/conbuildmat

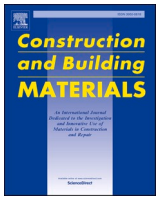

Improved flowability and strength using carbonated BOF slag and potassium citrate in sustainable LC3 binder

Zixing Liu [a], Yanjie Tang [a,b,*], K. Schollbach [a], H.J.H. Brouwers [a,b]

[a] Department of the Built Environment, Eindhoven University of Technology, Eindhoven 5600 MB, the Netherlands
[b] State Key Laboratory of Silicate Materials for Architectures, Wuhan University of Technology, Wuhan 430070, PR China

ARTICLE INFO

Keywords:
Ternary blends
Calcined low-grade Dutch clay
Potassium citrate
Carbonated BOF slag
Life cycle assessment

ABSTRACT

This study proposes a sustainable LC3 binder incorporating calcined low-grade clay, carbonated basic oxygen furnace slag (Cs), and potassium citrate (citrate) as a ternary cementitious system. Cs and citrate replace limestone powder (Ls) and polycarboxylate superplasticizer (SP), respectively. Citrate enhanced flowability while extending the hydration induction period, achieving up to a 9.1% increase in flow. Compared with SP-modified LC3, citrate improved compressive strength by 6.8–11.8%, while Cs incorporation further increased 28-day strength by up to 29.7%. Microstructural analyses revealed reduced porosity, refined pore structure, lower portlandite content, and increased C-S-H formation due to enhanced pozzolanic reactions. Life cycle assessment showed that Cs blends reduced CO_2 emissions and energy consumption by approximately 19%, demonstrating their potential as high-performance, low-carbon binders.

1. Introduction

Limestone Calcined Clay Cement (LC3) is a ternary blended cement that has been developed over the past decade as a sustainable alternative to conventional Portland cement. It incorporates up to 50% limestone and calcined clay as partial replacements for Portland cement clinker, significantly reducing associated CO_2 emissions [1,2]. This type of cement works well because of the combined effects of the pozzolanic reaction from calcined clay and the filler effect from limestone [1]. As a result, it allows for more clinker to be replaced, and it forms a finer microstructure. This gives the blended cement similar strength and durability to ordinary Portland cement (OPC) [3].

The performance of LC3 is largely influenced by the reactivity of the calcined clay used. Kaolinitic clay is the most commonly employed in LC3 systems [4,5] due to its high reactivity upon calcination at relatively low temperatures (600–900 °C), which is significantly lower than the temperatures required for clinker production (1400–1500 °C) [6]. Upon calcination, kaolinitic clay undergoes de-hydroxylation, forming metakaolin, which reacts with calcium hydroxide ($Ca(OH)_2$) to produce calcium alumina-silicate hydrates (C-A-S-H)—the primary binding phases in hydrated cement [7]. However, high-quality kaolinitic clay is relatively scarce and expensive, as kaolinite is also in high demand in other applications such as in paper and ceramics [8].

The use of locally available low-grade clays as alternatives to kaolinitic clay offers both economic and environmental advantages due to their greater abundance and lower cost [9]. Consequently, there is growing research interest in the effective utilization of such materials in LC3 systems. Although the composition of low-grade clays varies regionally, they are typically characterized by high contents of illite and montmorillonite, and lower kaolinite content (generally less than 40 wt. %) [10]. This results in reduced reactivity upon calcination. Each clay mineral has a distinct optimal calcination temperature—approximately 700 °C for kaolinite, 800 °C for montmorillonite, and 850 °C for illite—with kaolinite being the most reactive [10]. As a result, the use of low-grade clays as supplementary cementitious materials (SCMs) often leads to diminished early hydration kinetics and slower strength development [6,10,11]. This is primarily attributed to their lower availability of reactive silica and alumina, and higher iron content, which collectively reduce the amount of reactive phases formed under alkaline conditions.

To enhance the availability of reactive silica and alumina in LC3 systems, industrial by-products such as Basic Oxygen Furnace (BOF) slag—a waste material generated during steel production via the Linz-Donawitz process—present a promising alternative [12]. BOF slag has the potential to partially replace limestone as filler in cement, also promoting the formation of carboaluminates, and enhancing durability.

* Corresponding author at: Department of the Built Environment, Eindhoven University of Technology, Eindhoven 5600 MB, the Netherlands.
E-mail address: yanjie.tang@polyu.edu.hk (Y. Tang).

https://doi.org/10.1016/j.conbuildmat.2026.145232
Received 11 July 2025; Received in revised form 30 December 2025; Accepted 9 January 2026

However, its intrinsic hydraulic reactivity is limited due to impurities in belite (C_2S) and elevated iron content in calcium aluminoferrite (C_2(A, F)) phases [13]. Carbonation treatment of BOF slag significantly improves its reactivity by transforming C_2S into calcium carbonates and amorphous silica gel [14]. The carbonated slag mimics the role of limestone in blended cement by contributing to the filler effect, carboaluminate formation, and durability enhancement [14]. During carbonation, C_2S is primarily altered, while C_2(A, F) remains largely unaffected, thereby preserving its potential for continued reactivity [15]. Additionally, potassium citrate (citrate) has been proposed as a multifunctional admixture in such systems. Unlike conventional superplasticizers, citrate not only enhances workability but also activates iron-rich phases in BOF slag, improving reactivity and flowability [16]. Moreover, its iron-chelating properties may facilitate the dissolution of iron-bearing clays, further contributing to the reactivity of blended systems. Overall, the substitution of limestone powder (Ls) with carbonated BOF slag (Cs) in LC3 systems offers a promissing pathway for valorizing steelmaking waste while reducing reliance on quarried limestone [17]. Previous studies on LC3 systems have focused on either replacing calcined clay with other SCMs and pure metakaolin [18,19] or replacing Ls with other industrial by-products [20]. Moreover, in these LC3 systems, polycarboxylate superplasticizer (SP) [21] or naphthalene-sulfonate-based liquid superplasticizer [22] is commonly used as an admixture. However, the use of Cs as a substitute for Ls and citrate as a superplasticizer remains scarcely explored. Cs not only stabilizes free lime and periclase but also introduces reactive carbonates that can actively participate in hydration [14]. Citrate has been studied primarily as a chelating agent or setting modifier; however, to the authors' knowledge, its application as an alternative to conventional SP in LC3 systems has not been reported yet.

To investigate the effects of using citrate as a superplasticizer and Cs as a partial replacement for Ls in ternary cement blends, a comparative study was conducted against a reference LC3 system containing calcined low-grade Dutch clay. The reference composition employed conventional Ls as a filler and a standard superplasticizer to optimize water demand. This paper specifically examined how varying citrate dosages and the substitution of Ls with Cs influence phase development, microstructural evolution, and mechanical performance. A comprehensive suite of characterization techniques was employed, including X-ray diffraction (XRD), thermogravimetric and differential thermogravimetric analysis (TG/DTG), isothermal calorimetry, porosity analysis, and mechanical strength testing. In addition, leaching tests and life cycle assessment (LCA) were conducted on the final hardened materials to evaluate their environmental footprint and long-term stability.

2. Experimental study

2.1. Raw materials

Ordinary Portland cement (CEM I 52.5 R, the mineral composition of clinker includes: C_3S: 62%, C_2S: 10.2%, C_3A: 8.1%, C_4AF: 8.4%) was supplied by Heidelberg Materials (Germany) and used as the primary binder in this study. BOF slag was obtained from Tata Steel in IJmuiden, the Netherlands, while the low-grade clay was sourced from TCKI in Velp, also located in the Netherlands. The chemical compositions of the cement, clay, and BOF slag were determined using X-ray fluorescence (XRF) spectroscopy (PANalytical Epsilon 3), following the fused bead method, which is presented in Table 1. Cs was prepared through a controlled carbonation process. Initially, the slag was ground using a disc mill (Retsch RS300XL) for 15 min to obtain a fine powder. The powdered slag was then moistened by spraying with distilled water at a water-to-solid ratio of 0.1. Subsequently, the mixture was placed in a 240 L climate chamber and subjected to carbonation for 72 h at 20 °C, with a relative humidity of 80% and a CO_2 concentration of 20% [15]. After 72 h of carbonation, the BOF slag exhibited no visible color change upon application of a 0.5% phenolphthalein solution, indicating complete carbonation. To remove residual moisture, the Cs was oven-dried at 105 °C for 24 h, followed by regrinding for 5 min to break up agglomerated particles. The mineralogical compositions of both uncarbonated and carbonated BOF slag are presented in Table 2. As shown in Table 2, a significant reduction of C_2S after carbonation can be seen. This indicates that carbonation consumes part of the reactive silicate phases, leading to secondary carbonate formation and improved stability. Carbonates (calcite, aragonite) can act as fillers and improve microstructure densification [14]. Furthermore, carbonation generates more amorphous products (e.g., $CaCO_3$ polymorphs, C–S–H gels disrupted into non-crystalline products) [15]. This can enhance reactivity in blended cement systems. The low-grade Dutch clay was found to contain a mixture of minerals, including quartz (SiO_2, silicon dioxide), kaolinite ($Al_2Si_2O_5(OH)_4$), illite ((K, H_3O)(Al, Mg, Fe)$_2$(Si, Al)$_4O_{10}$[(OH)$_2$,(H_2O)]), nacrite (a kaolinite-type polymorph), wüstite (FeO), which contributes to the clay's elevated iron content, and montmorillonite ((Na, Ca)(Al, Mg)$_6$(Si_4O_{10})$_3$(OH)$_6$-nH_2O, a member of the smectite group and a 2:1 clay). The particle size distribution (PSD) of the Ls, calcined low-grade Dutch clay, Cs, and Portland cement is illustrated in Fig. 1. Two admixtures were used in this study: (1) citrate ($K_3C_6H_5O_7 \cdot H_2O$, analytic grade) and (2) a SP with a 30% water reduction rate, industrial grade. Both admixtures are commercially available.

Table 1
The chemical composition of the Portland cement, low-grade Dutch clay, and BOF slag.

Properties		Cement	Clay	BOF slag
Chemical composition (wt.%)	SiO_2	15.81	66.63	13.45
	Al_2O_3	6.87	16.93	2.21
	Fe_2O_3	3.74	10.11	28.32
	CaO	66.83	0.93	40.14
	MgO	1.17	0.57	6.8
	SO_3	3.07	/	/
	K_2O	0.24	3.18	/
	TiO_2	0.44	1.09	1.39
	P_2O_5	/	/	1.61
	V_2O_5	/	/	1.05
	Cr_2O_3	/	/	0.3
	MnO	/	/	4.61
	Others	1.83	0.56	0.12
	L.O.I	0.92	5.43	/
	G.O.I	/	/	1.31
Density (g/cm^3)		3.03	2.51	3.60
Specific surface area (m^2/g)(Before calcination/carbonation)		1.50	23.14	1.34
Specific surface area (m^2/g) (After calcination/carbonation)		/	14.19	6.03
Kaolinite content (wt.%)		/	14.80	/
Median size (d_{50})		8.42	16.44	12.83

2.2. Clay calcination

The raw clay was first oven-dried at 105 °C for 24 h to remove moisture [10]. Following drying, the material was ground using a disc mill for 3 min to obtain a uniform powder. To enhance its pozzolanic

Table 2
The mineralogical composition of BOF slag and Cs.

Phase (wt.%)	BOF slag	Carbonated BOF slag
C_2(A, F)	17.1	17.8
Magnetite	6.4	5.8
C_2S	39.6	19.8
Wüstite	20.7	24.8
Lime	0.8	0.7
Calcite	0.7	4.7
Aragonite	/	0.5
Portlandite	0.7	/
Amorphous	14.0	25.9

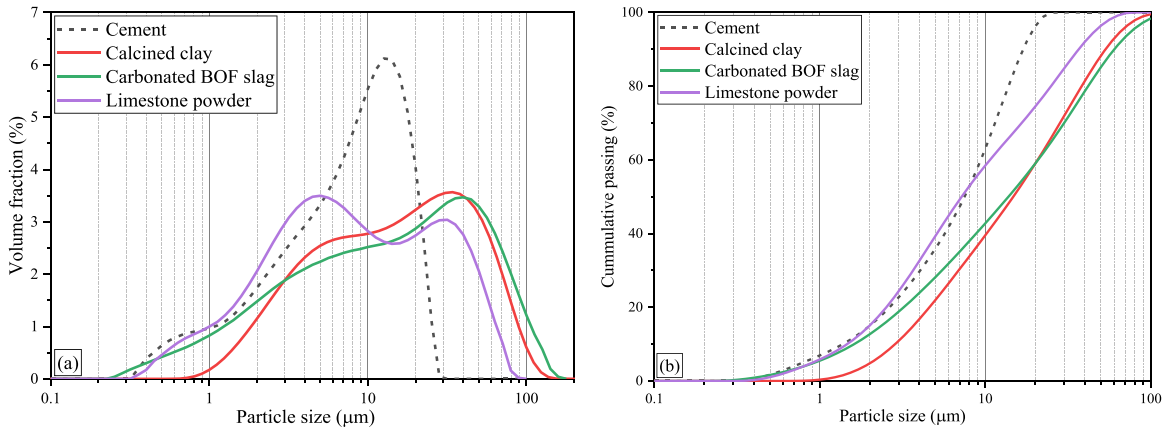

Fig. 1. Particle size distributions of cement, calcined clay, limestone powder (Ls), and carbonated BOF slag (Cs).

reactivity, the clay powder was thermally activated in a muffle furnace at 800 °C [5]. In industrial practice, a calcination temperature range of 750–800 °C is commonly employed due to its efficacy in achieving optimal reactivity [23]. The temperature was ramped up at a rate of 5 °C/min until it reached 800 °C, where it was held for 2 h to ensure complete calcination [10]. After the heating process, the calcined clay was allowed to cool to room temperature under ambient conditions. The color change of the clay before and after calcination is shown in Fig. 2. During the cooling process in air, oxidation of wüstite can happen after dropping below 650 °C, imparting the characteristic reddish color to the calcined clay [24], as shown in Fig. 2.

2.3. Separation of the silt and clay fractions for X-ray powder diffraction by centrifugation

The details of clay separation are shown in Appendix A. Supplementary data.

2.4. Mixture proportions

The mixture designs used in this paper are summarized in Table 3. All ternary blends were prepared with a constant water-to-binder ratio (W/B) of 0.5 and a norm sand-to-binder ratio (S/B) of 3. The reference mixture, corresponding to a typical LC3 formulation, consisted of 50 wt.% OPC, 30 wt.% calcined low-grade Dutch clay, and 20 wt.% Ls. Both citrate and SP were incorporated at a dosage of 0.1 wt.% of the total binder mass, a commonly adopted value in cement research. To evaluate the effect of enhanced activation of iron-rich phases in BOF slag, an additional mixture containing a higher citrate dosage (0.25 wt.%) was also prepared. Prior to mixing, the chemical admixtures (citrate and SP) were dissolved in the mixing water to ensure uniform distribution. Mortar specimens were cast in standard prismatic molds (40 mm × 40 mm × 160 mm), following the procedure specified in BS EN 196–1 [25]. After casting, samples were covered with plastic film and cured under ambient air conditions for 7 and 28 days. In parallel, cement pastes with the same W/B ratio (0.5) were produced for microstructural analysis at the same curing ages. After curing, the paste samples were crushed and stored in sealed plastic containers at 20 °C in a desiccator containing calcium chloride (as a desiccant) and sodium hydroxide pellets to minimize carbonation.

2.5. Methods

2.5.1. Analytic technologies

The particle size distribution (PSD) of the raw materials was analyzed using a laser diffraction particle size analyzer (Mastersizer 2000, Malvern Instruments). The mineralogical compositions of both raw materials and hydrated blended cement pastes were characterized using two primary techniques. First, XRD analysis was performed using a D4 ENDEAVOR diffractometer (Bruker) equipped with a LynxEye detector. Scans were conducted over a 2θ range of 5° to 90°, with a step time of 1 s. Second, TG analysis was conducted using a Jupiter STA 449 F1 thermal analyzer (Netzsch). The samples were heated from 40 °C to 1000 °C at a constant rate of 10 °C/min under a nitrogen atmosphere. To determine the amount of kaolinite in the raw clay, the mass loss between 400 and 600 °C was analyzed using the tangent method. The calculation followed the equation:

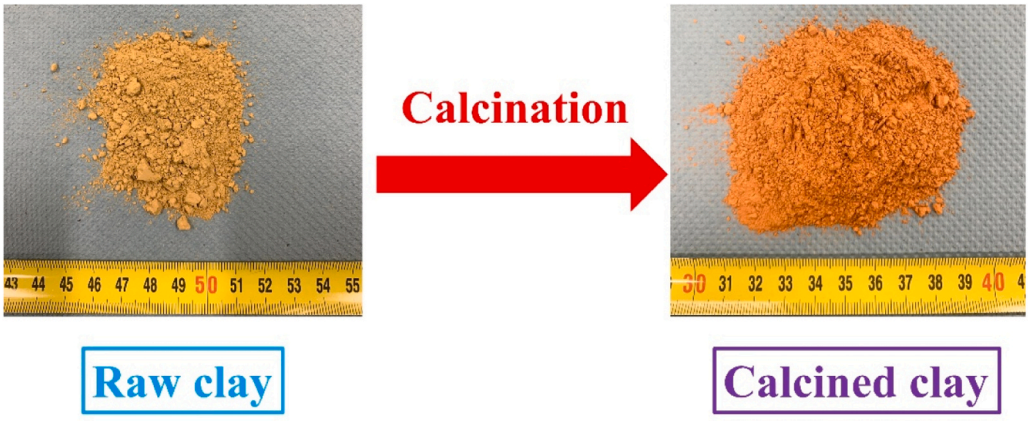

Fig. 2. The color change of clay before and after calcination.

Table 3
Mix designs of mortar samples.

Mixture	Admixtures content (wt.%)	Cement (g)	Ccl (g)	Cs (g)	Ls (g)	Water (g)	Sand (g)	Flowability (mm)
CsCit	0.1	225	135	90		225	1350	170.0
CsHCit	0.25	225	135	90		225	1350	190.0
Cs	0.1	225	135	90		225	1350	162.5
LsCit	0.1	225	135		90	225	1350	180.0
LsHCit	0.25	225	135		90	225	1350	197.5
Ls	0.1	225	135		90	225	1350	165.0

Note: Cs denotes the carbonated BOF slag; Ccl denotes the calcined clay; Ls denotes the limestone powder; Cit denotes potassium citrate. The groups named Cs and Ls use SP as an admixture. The value of flowability is an average measurement value.

$$wt.\%_{kaolinite} = wt.\%_{kaol-OH}\frac{M_{kaolinite}}{2m_{water}} \quad (2)$$

Here,$wt.\%_{kaol-OH}$ denotes the mass loss during the de-hydroxylation process; $wt.\%_{kaolinite}$ denotes the content of kaolinite; $M_{kaolinite}$ and $2m_{water}$ denotes the kaolinite and water molecular weight, respectively.

Calorimetric measurements were performed using an isothermal calorimeter (TAM Air, Thermometric) at a constant temperature of 20 °C over a period of 7 days to monitor the heat evolution associated with hydration. Porosity was evaluated by Mercury Intrusion Porosimetry (MIP) using an Autopore IV 9500 porosimeter (Micromeritics), with a mercury filling pressure of 0.0141 MPa and an equilibration time of 20 s. The results interpretation employed a surface tension of 485 mN/m for mercury (γ_{Hg}) and a contact angle (θ) of 130° [26]. Prior to the MIP test, samples that had undergone 28 days of hydration were cut into 3 mm cubes, immersed in isopropyl alcohol for 7 days, and then dried in a desiccator for an additional 3 days. In addition, the specific surface area of the raw materials and the porosity of the hydrated products were determined using Brunauer–Emmett–Teller (BET) nitrogen adsorption analysis (TriStar II, Micromeritics). All samples underwent automatic degassing at 40 °C with a ramp rate of 10°C/min over a period of 2 h. Only the adsorption branch of the isotherm was considered in the analysis to eliminate errors arising from tensile strength effects and to avoid misinterpretation of pore structure characteristics, as recommended in previous studies [27]. Additionally, Fourier Transform Infrared Spectroscopy (FTIR) was employed to investigate the chemical changes in BOF slag before and after carbonation. The FTIR measurements were conducted with a resolution of 4 cm^{-1}, a data interval of 1 cm^{-1}, and an accumulation of 20 scans to ensure signal clarity and reproducibility. To observe the morphology of the hydration products, a Thermo Scientific Phenom Desktop scanning electron microscope (SEM) was used to perform SEM analysis on 28-day hydrated pastes. Prior to analysis, samples were gold-plated using an Emitech K550X coating machine (current: 30 mA, coating time: 30 s).

2.5.2. Workability

In this study, the three specimens in each mix design undergo a uniform flowability test method twice prior to casting. In accordance with EN 1015–3, the average of the two test diameters is recorded using a standard conical ring, and the flowability enhancement ratio [28] is calculated using the following equation:

$$\textit{The flowability enhancement ratio}\ (\%) = \frac{d_{LC3-Ls} - d_{LC3-cs}}{d_{LC3-Ls}} \times 100\% \quad (3)$$

Here, d_{LC3-Ls} denotes the slump flow of mortar containing Ls; d_{LC3-cs} denotes the slump flow of mortar containing Cs. In both ternary blends, the same admixtures: citrate (0.1 and 0.25 wt.%) and SP (0.1 wt.%) were considered.

2.5.3. Mechanical performance of mixed mortars

The compressive strength of the blended cement mortars was evaluated after 7 and 28 days of curing. Measurements were performed on three specimens per mix, using the broken halves obtained from standard three-point bending tests, in accordance with BS EN 196–1. This approach ensured consistent sample dimensions and reliable mechanical property assessment.

2.5.4. Environmental impact evaluation

A one-stage batch leaching test was conducted on mortar samples cured for 28 days, in accordance with the EN 12457–2 standard. The cured mortar was crushed into particles smaller than 4 mm and subjected to a dynamic shaker at ambient temperature for 24 h, using a liquid-to-solid ratio of 10:1 and a shaking speed of 250 rpm. The resulting leachate was filtered through a membrane filter with 0.017–0.030 μm. Following filtration, the leachate was acidified with nitric acid (HNO_3), and elemental concentrations were determined using Inductively Coupled Plasma Optical Emission Spectrometry (ICP-OES, SPECTROBLUE). The obtained concentrations were compared against the threshold values specified by the Dutch Soil Quality Decree [12].

2.5.5. CO_2 emissions and energy consumption

In accordance with ISO 14040 and 14044 guidelines, an LCA comprises four primary phases: (1) definition of system boundaries, (2) inventory analysis, (3) impact assessment, and (4) interpretation of results [29–31] was used. In this study, the LCA focused on evaluating the environmental impacts associated with the production of raw materials used in the cementitious blends. The primary environmental concerns in concrete construction are the depletion of natural resources and the emission of CO_2, which significantly contributes to global warming [31]. The use of locally sourced, abundant raw materials with lower energy demands can help mitigate these impacts, which can produce more durable concrete, enhance long-term sustainability. Therefore, the LCA methodology was employed to estimate both CO_2 emissions and energy consumption for each mixture. The analysis was conducted using SimaPro software, following the procedures described in detail in [31].

3. Results and discussion

3.1. Characterization of the raw material

Although the de-hydroxylation of illite and montmorillonite occurs over a broad temperature range, it predominantly takes place between 600 °C and 900 °C [11]. In this study, the kaolinite content of the clay was determined to be approximately 14.80 wt.%, according to Eq. (2), as presented in Table 1. The corresponding mass loss at various temperature intervals is summarized in Fig. 3. The evaporation of the water adsorbed on the clay surface, and the inter-layer water occurred before 250 °C [10]; The decomposition of iron oxyhydroxides occurred between 250 and 350 °C [10]; The de-hydroxylation of kaolinite to form metakaolin occurred between 350 and 600 °C [32]; The de-hydroxylation of montmorillonite occurred between 650 and 900 °C [10]. The total mass loss observed between 350 and 950 °C is attributed to the de-hydroxylation of clay minerals [32], which is further supported by the XRD analysis results shown in Fig. 4.

The XRD patterns of the raw and calcined clay after separation are presented in Fig. 4. The characteristic diffraction peaks of kaolinite disappear after calcination at 800 °C, indicating the transformation of the crystalline kaolinite phase into an amorphous phase, commonly

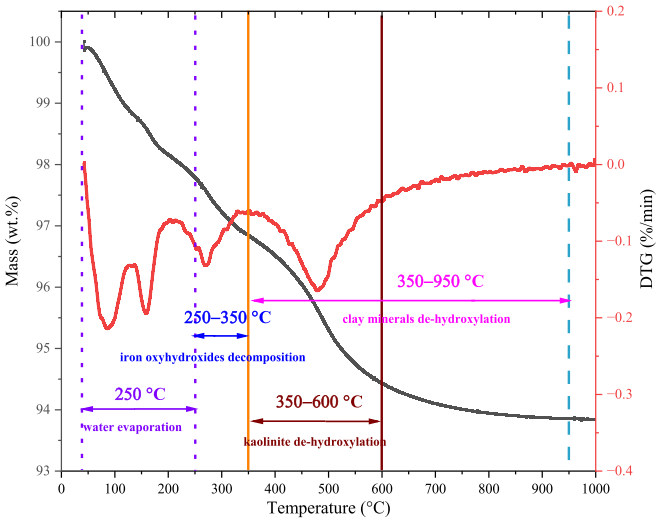

Fig. 3. TG analysis of low-grade clay.

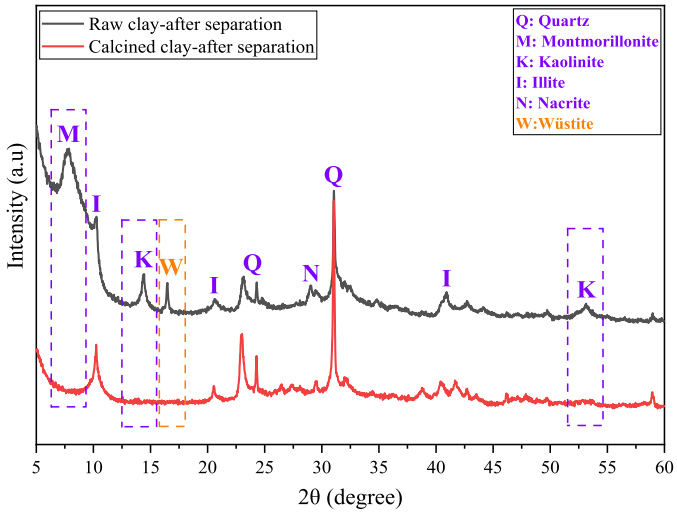

Fig. 4. XRD patterns of the raw and calcined clay after separation.

referred to as metakaolin. This similar behavior was also observed at montmorillonite, as its characteristic diffraction peak at 7° (2θ) becomes absent [23]. De-hydroxylation of the clay, i.e., the removal of hydroxyl (OH^-) groups, occurs primarily between 350 °C and 850 °C, leading to structural disorder and thereby the formation of amorphous [10,33].

The FTIR spectra of BOF slag before and after carbonation are shown in Fig. 5. A notable shift in the Si–O stretching vibration band from 916 cm^{-1} to 1061 cm^{-1} indicates the formation of silica gel, which can enhance the pozzolanic reactivity of the material [34]. Additionally, the significant increase in the intensity of the absorption band near 1410 cm^{-1}, corresponding to the asymmetric stretching mode of carbonate (CO_3^{2-}) groups, confirms the formation of substantial amounts of $CaCO_3$ during carbonation [34].

3.2. Flowability of fresh mortars

Fig. 6 illustrates the influence of different admixtures on the flowability of ternary cement mortars. It is well established that calcined clay increases water demand due to its high surface area and adsorption capacity [5]. The LsHCit sample exhibited the highest flowability at 197.5 mm, while the Cs sample showed the lowest flowability at 162.5 mm. In general, ternary mortars containing Ls demonstrated

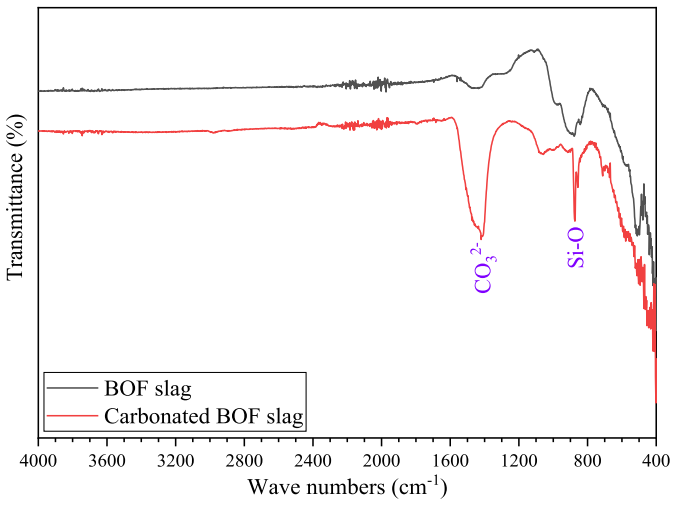

Fig. 5. FTIR absorption spectra of BOF slag before and after carbonation.

better flowability, consistent with the mixture compositions in Table 3, than those incorporating Cs. This difference can be attributed to the lower specific surface area of Ls (0.96 m^2/g) compared to Cs (6.03 m^2/g). The blend incorporating Ls and 0.1 wt.% citrate (LsCit) exhibited a 9.1 % increase in flowability relative to the sample modified with SP alone (Ls). Furthermore, the flowability enhancement ratios, presented in Fig. 6(a), show relatively small variations, suggesting that the primary factor influencing flowability is the type and dosage of admixtures. As seen in Fig. 6(b), flowability improves with increasing citrate content. In contrast, increasing the citrate content from 0.1 to 0.25 wt.% led to the highest enhancement (11.8 %) in the flowability of the blend containing Cs.

3.3. Hydration

3.3.1. Hydration kinetics

The isothermal conduction calorimetry results for the ternary blend pastes are presented in Fig. 7. Among the mixtures, the Ls group displays a more pronounced exothermic peak compared to blends incorporating Cs. This is likely due to limestone's role as a nucleation site for hydration products and as a physical filler [35–37]. Although Cs contains considerable amounts of calcium carbonate and silica gel, a delay in hydration was observed. This delay is attributed to the release of heavy metals such as vanadium (V), predominantly associated with C_2S and liberated during carbonation [14]. Previous studies have indicated that V can delay the hydration process of OPC samples by several hours [14,38]. This effect may similarly cause cement hydration delay in the present study. The effect of Cs on cement hydration can be attributed to simultaneously accelerating the hydration reactions of silica gel and calcium carbonate, while V exerts a retarding effect. Furthermore, the induction period was longer in the groups containing citrate compared to those with the SP, and this extension became more significant with increased citrate dosage (from 0.1 to 0.25 wt.%). This trend aligns with citrate's known function as a hydration retarder, the influence of which depends on both dosage and water-to-cement ratio [12]. Notably, despite the observed retardation, the cumulative hydration heat increased in the systems containing either Cs or citrate. This can be explained by the pozzolanic reaction between the silica gel present on the surface of the Cs and the portlandite produced during cement hydration, as well as the activating effect of citrate on iron-rich phases in the system [12,39].

3.3.2. Phase identification

The XRD results of the ternary blends at 7 and 28 days are presented

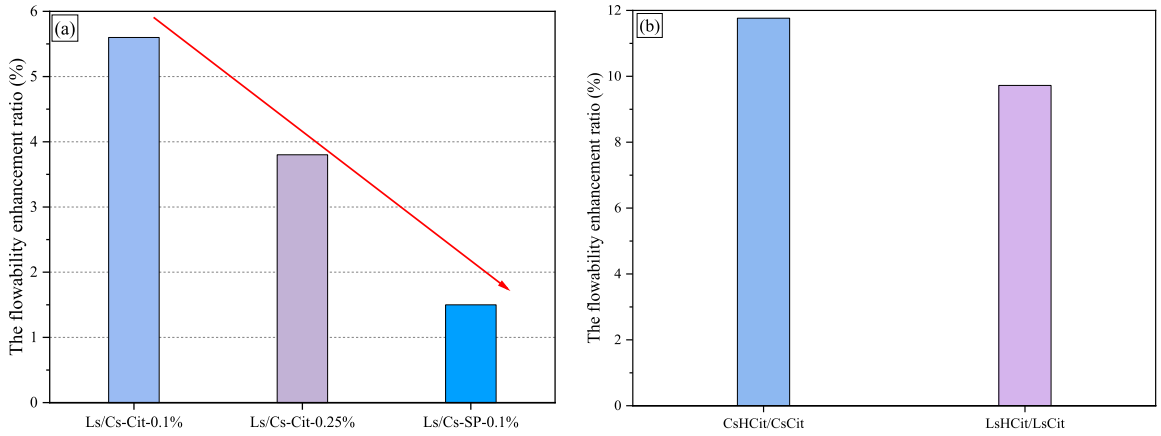

Fig. 6. (a) The flowability enhancement ratio of different ternary blends; (b) The flowability enhancement ratio of different contents of citrate.

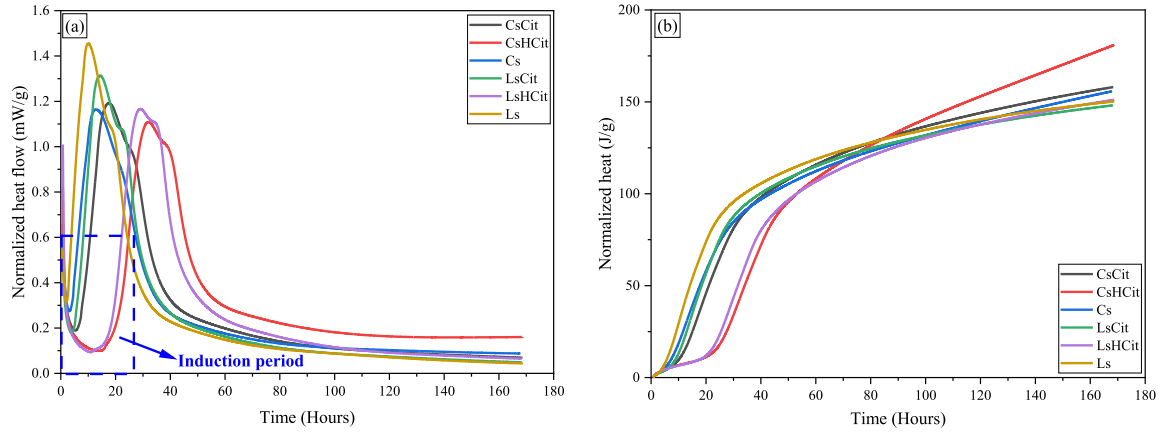

Fig. 7. Heat flow and cumulative heat evolution of ternary blends.

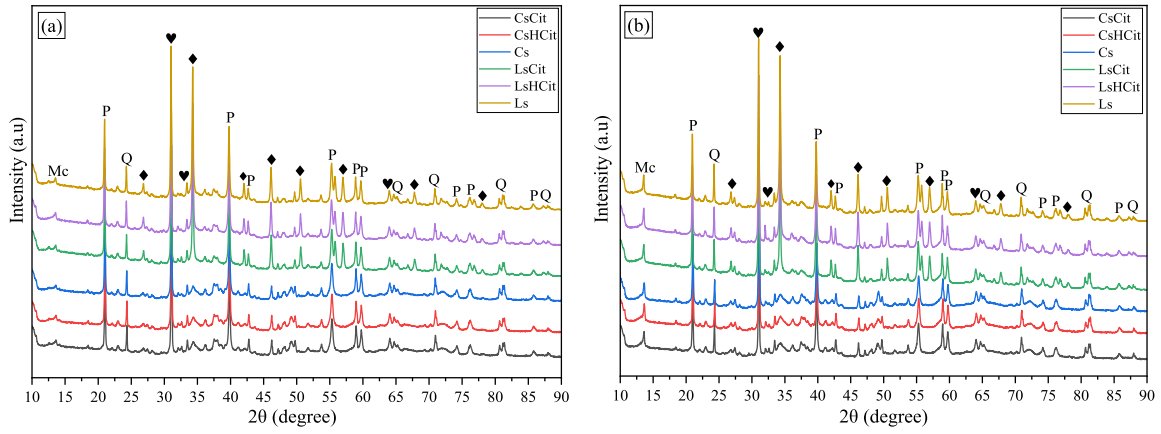

Fig. 8. Hydration products of ternary blends: (a) 7 days; (b) 28 days (Mc-monocarboaluminate; P-portlandite; Q-quartz; ◆-calcite; ♥-calcium silicate hydrate).

in Fig. 8. The primary hydration products identified include calcium hydroxide (portlandite), calcium silicate hydrate (C–S–H) gel, and a minor quantity of monocarboaluminate (Mc), all of which are typical in hydrated cementitious systems [40–43]. Quartz was consistently detected in all ternary blends, attributed to its chemically inert nature. SCMs such as calcined clay and Cs participate in pozzolanic reactions, where portlandite is consumed to generate additional C–S–H gel. However, these transformations are often not clearly discernible in XRD due to the amorphous nature of the secondary phases formed. Therefore, such changes are more effectively observed through TG analysis, as elaborated in Section 3.3.3. In blends containing Ls, sharp diffraction peaks corresponding to calcite were visible, reflecting the crystalline nature of the limestone. In contrast, while BOF slag also forms calcite during carbonation, its content becomes significantly diluted upon blending, rendering its characteristic diffraction peaks less prominent in the XRD patterns.

3.3.3. TG analysis

TG analysis of the hydration products in the ternary blends at 7 and 28 days is presented in Fig. 9. The decomposition profile of the ternary systems closely follows that of conventional hydrated cementitious materials, comprising three main stages: (i) mass loss between 40–390 °C, attributed to the dehydration of C-S-H and aluminate-containing phases; (ii) a distinct weight loss between 390–460 °C, corresponding to the decomposition of portlandite; and (iii) mass loss between 500–800 °C, associated with the thermal decomposition of calcium carbonates [42], as summarized in Table 4. At 28 days, the Cs group exhibited a lower portlandite content compared to the Ls group, primarily attributed to the consumption of portlandite by the newly formed silica gel during the ongoing pozzolanic reaction. This reaction is further evidenced by the increased mass loss in the Cs group in the lower temperature range (40–390 °C), suggesting the formation of additional C-S-H gel. Moreover, compared to the blends containing Ls, the decomposition of calcium carbonates in the blends incorporating Cs occurs at relatively lower temperatures (650–700 °C) compared to that of calcite (750–900 °C). This observation suggests the presence of metastable carbonate phases, such as aragonite and vaterite, which are thermodynamically less stable than calcite and may not be readily detected by XRD due to their low crystallinity and content [44].

Table 4
The mass loss of LC3 at 7- and 28-day curing.

Mixture	Mass loss (wt.%)					
	40–390 (℃)		390–460 (℃)		500–800 (℃)	
	7 d	28 d	7 d	28 d	7 d	28 d
CsCit	9.08	10.89	1.69	1.29	3.12	3.75
CsHCit	6.74	11.45	0.55	1.54	6.45	3.53
Cs	8.74	10.90	1.79	1.57	3.03	3.35
LsCit	8.72	9.65	2.15	1.90	9.14	9.58
LsHCit	8.88	9.94	1.53	1.94	9.80	9.43
Ls	8.45	10.58	2.08	1.89	9.61	9.27

3.4. Feasibility evaluation of ternary blended cement mortars

3.4.1. Mechanical performance and microstructure

The compressive strength of the ternary blends after 7 and 28 days of curing is shown in Fig. 10(a). Notably, blends incorporating Cs exhibited higher compressive strengths than those containing Ls at both curing ages. The incorporation of Cs enhanced 28-day compressive strength by 23.9% and 29.7% relative to conventional LC3 systems using 0.1 wt.% citrate and SP. This trend aligns with the TG analysis results, which revealed a greater quantity of chemically bound water in the BOF slag-containing samples, indicating more extensive hydration. Several factors contribute to the enhanced performance of blends with Cs. First, the rough and porous surface morphology of the slag particles improves mechanical interlocking and bond strength at the paste–aggregate interface [15]. Second, the higher water absorption capacity of Cs reduces the amount of free water in the fresh mix, which enhances early strength. Over time, the absorbed water can be gradually released, acting as an internal curing agent that promotes continued hydration of the cement matrix [15]. Furthermore, the incorporation of citrate led to an increase in compressive strength compared to the use of SP, for both 7- and 28-day curing periods. After 28 days of curing, the compressive strength of citrate-modified samples increased by 6.8% and 11.8% compared to their SP-modified counterparts. This improvement is likely due to citrate's ability to chemically activate iron-bearing phases, an effect particularly pronounced in blends containing Cs. Supporting this observation, the cumulative hydration heat in the Ls-containing blends

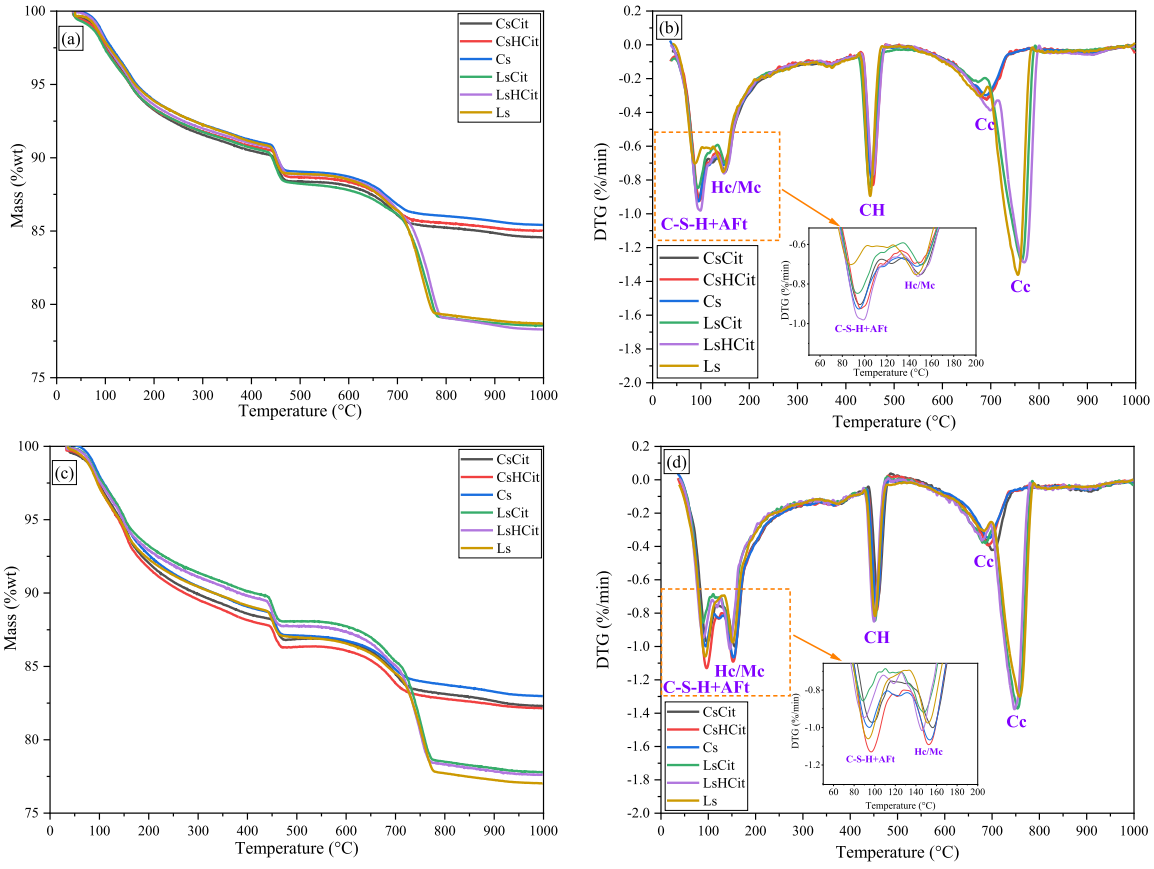

Fig. 9. TG analysis of ternary blends: (a)-(b) 7 days; (c)-(d) 28 days (Hc: hemi-carboaluminate, Mc: mono-carboaluminate, AFt: Ettringite, CH: portlandite, Cc: calcite).

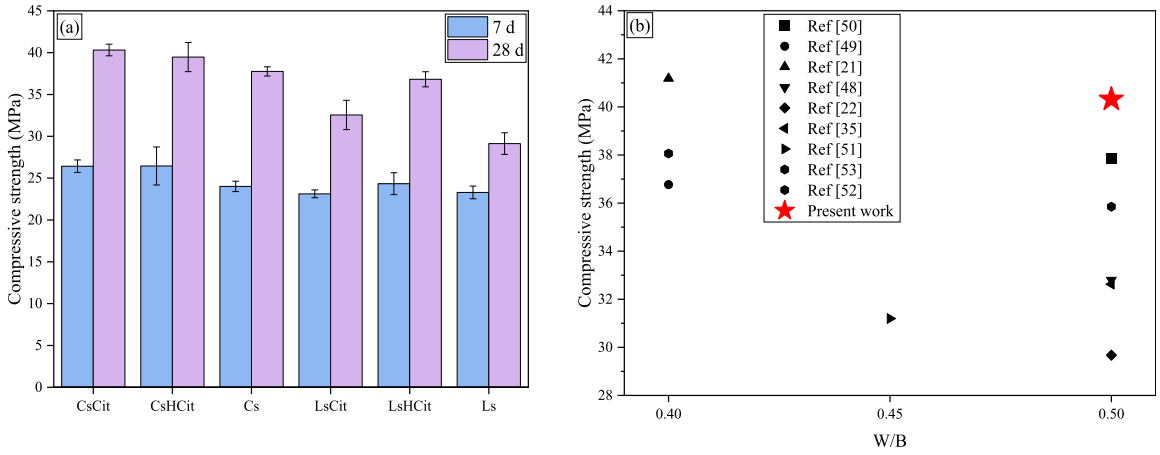

Fig. 10. The compressive strength of ternary blends. (a) The results in the present work, (b) The compressive strength of LC3 from other scholars and the present work at 28 days for comparison.

remained relatively consistent regardless of citrate dosage, while Cs-containing blends showed increased heat release with higher citrate content. These results highlight the dual functionality of citrate in LC3 systems, where it acts both as a water-reducing agent and a chemical activator. Its activation potential is especially effective in systems incorporating iron-rich industrial by-products such as BOF slag, as opposed to more inert materials like limestone. Similar findings reported in the literature affirm that citrate, despite its known retarding effect on early hydration, can significantly enhance long-term strength development when used in appropriate dosages [45–47].

Fig. 10(b) and Table 5 present a comparative analysis of various LC3 systems reported in the literature, focusing on admixture types and dosages, W/B ratios, and kaolinite contents. To maintain consistency, the reported data represent the mean values of the optimal mixtures from each study. The clay used in the present work had a relatively low kaolinite content (14.8 wt.%) compared to other references. Despite this drawback, the ternary blends incorporating Cs achieved slightly higher 28-day compressive strength than those reported in the literature with comparable W/B ratios. Remarkably, under identical W/B conditions (0.4), the ternary blends containing citrate in the present work outperformed those investigated by Liu et al. [48], who utilized clay with a higher kaolinite content (28.4 wt.%) and SP rather than citrate. Furthermore, the 28-day compressive strength of the blends incorporating Cs also exceeded that reported by Avet et al. [49], despite their use of a lower W/B ratio (0.4) and a higher SP dosage (1.4 wt.%). The results also indicated that a citrate dosage of 0.25 wt.% provided the most favorable balance between flowability improvement and strength development. From an economic perspective, the cost of citrate is generally higher than that of conventional SP. However, citrate offers additional benefits: it is biodegradable, derived from renewable resources, and simultaneously enhances flowability while moderating the hydration kinetics of the LC3 system. Thus, although its cost may limit widespread use in standard concrete applications, citrate may be particularly suitable for sustainable or specialty binders where environmental compatibility and multifunctional performance are prioritized. These findings underscore the effectiveness of Cs as an SCM and highlight the superior performance of citrate as a multifunctional admixture. The combination of these materials enabled the production of high-strength LC3 mortars, even with low-reactivity clay, indicating the potential for broader application using locally available and industrial by-product resources.

Fig. 11 presents the pore size distribution of the ternary blends as determined by nitrogen adsorption. Following the classification proposed by Zhang et al. [54], the measured pore sizes were divided into two key ranges to better understand the evolution of porosity with curing time: gel pores (2–10 nm) and microcapillary pores (10–100 nm). Gel pores are particularly significant, as they are closely associated with the formation of C-S-H, which is the binding phase responsible for mechanical strength in cementitious systems [55]. The results show that the Cs group exhibited a higher gel pore area compared to the Ls group, suggesting more extensive C-S-H formation and thus enhanced strength development. This observation is further supported by MIP results shown in Fig. 12 and summarized in Table 6. The Cs group displayed a lower total porosity (31.09%) compared to the Ls group (33.09%), indicating a denser microstructure. The findings of SEM results also confirm that the incorporation of Cs and citrate promotes refined pore structure and contributes positively to the mechanical performance of ternary blends, as shown in Fig. 13.

3.4.2. *Environmental impact evaluation*

A one-stage batch leaching test was conducted to assess the environmental impact of the ternary blends after 28 days of curing, with

Table 5
The type of admixtures in LC3 from other scholars and the present work.

Authors	Years	Admixtures	Content (wt.%)	Kaolinite content (wt.%)	W/B	Flowability (mm)
Ref [50]	2018	polycarboxylate superplasticizer	0.6	17	0.5	N/A
Ref [49]	2018	polycarboxylate superplasticizer	1.4	17	0.4	N/A
Ref [51]	2020	polycarboxylate superplasticizer	0.88	60	0.45	N/A
Ref [21]	2021	polycarboxylate superplasticizer	0.1–0.39	19.4	0.4	N/A
Ref [48]	2021	polycarboxylate superplasticizer	0.04–0.15	28.4	0.5	N/A
Ref [22]	2021	Naphthalene-sulfonate-based liquid superplasticizer	24	N/A	0.5	55–70
Ref [35]	2022	polycarboxylate superplasticizer	0.15	N/A	0.5	240–247
Ref [52]	2022	polycarboxylate superplasticizer	0.111	20.8	0.4	N/A
Ref [53]	2023	polycarboxylate superplasticizer	N/A	55	0.5	68–133
Present work	2025	polycarboxylate superplasticizer potassium citrate	0.1–0.25	14.8	0.5	162.5–197.5

Note: The content of admixtures is calculated by the mass of binders/solids; N/A denotes not available.

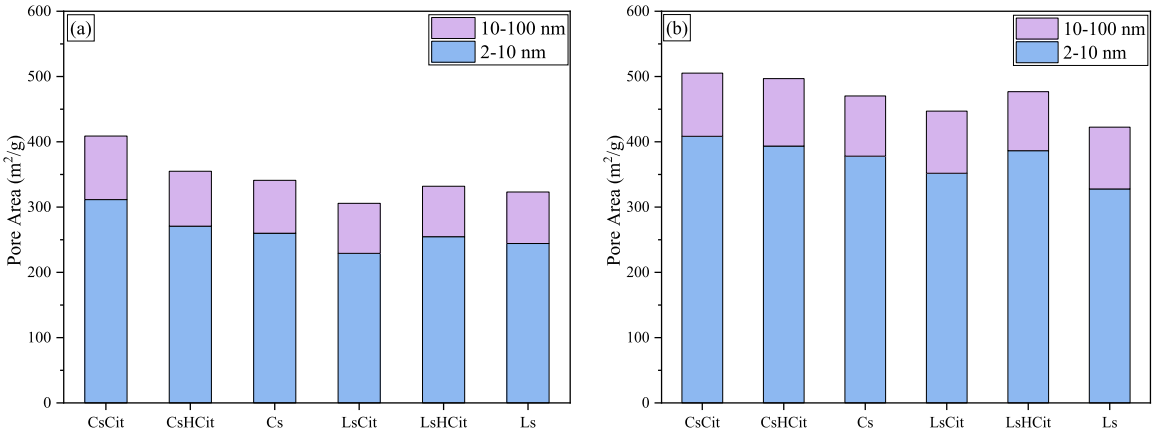

Fig. 11. Pore size classification (determined by BJH analysis of nitrogen adsorption isotherms) of ternary blends after: (a) 7 days and (b) 28 days.

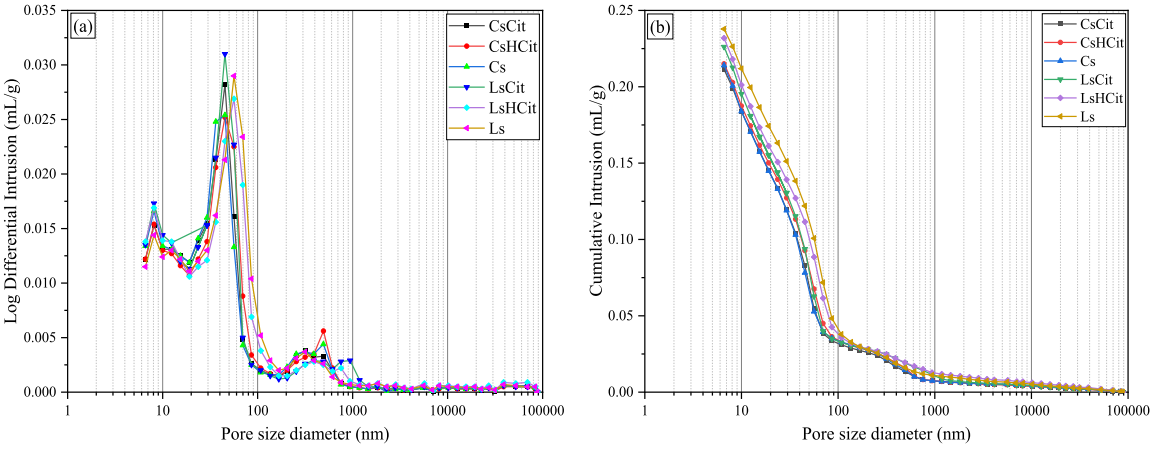

Fig. 12. Pore size distribution (determined by MIP) of ternary blends after 28 days of hydration.

Table 6
The porosity and average pore diameter of ternary blends after 28 days of curing.

Mixture	Porosity (%)	Average pore diameter (nm)
CsCit	31.43	20.5
CsHCit	31.67	21.2
Cs	31.09	20.0
LsCit	32.62	20.5
LsHCit	33.07	21.5
Ls	33.09	23.5

results summarized in Table 7. In general, hydrated cementitious systems are known to stabilize potentially harmful ions, providing environmental benefits in built environments. In this study, particular attention was given to chromium (Cr) and vanadium (V), which are the primary heavy metals present in the BOF slag used, and which may pose long-term leaching risks in slag-based construction materials [12]. V leaching was reduced mainly by immobilization within hydration products of the cementitious system [56]. When slag, calcined clay, or other aluminosilicate phases are present, they generate secondary hydrates such as C-S-H, AFm, and hydrotalcite-like phases. These provide sites for sorption, incorporation, or precipitation of V species (especially V^{5+}), effectively lowering their mobility. In addition, the high pH of the pore solution stabilizes V in less soluble forms, while carbonation or further hydration can encapsulate it within the solid matrix [56]. According to Vollpracht et al. [57], C-S-H gels have the ability to immobilize Cr ions. While Cr—the second most prevalent heavy metal in the BOF slag was detected in the leachate, its concentration remained well below the regulatory limits specified by the Dutch Soil Quality Directive (SQD). Similarly, V leaching was effectively mitigated. Since V leaching is highly sensitive to pH and tends to increase under acidic conditions, the inherently high alkalinity of the cement matrix likely played a key role in suppressing its release. Previous studies [58,59] have shown that while carbonation reduces alkalinity, the decrease is often limited to the exposed surfaces, and the inner matrix can retain a high pH for extended periods, particularly in dense cementitious systems with low permeability. Moreover, secondary phases such as C-S-H and AFm phases can continue to provide binding sites for metal ions even at moderately reduced pH levels. Therefore, the immobilization performance is anticipated to remain stable in the long term, though further accelerated carbonation or long-term leaching tests would be needed to confirm this behavior. These findings indicate that the ternary blends incorporating Cs demonstrate favorable environmental performance with respect to heavy metal stabilization and leaching behavior, thus supporting their safe application in construction.

3.4.3. LCA analysis

In this study, the environmental impacts associated with the production of raw materials were assessed using an LCA approach. The life cycle inventory data for sand, cement, calcined clay, Ls, Cs, and water were sourced from the SimaPro software database. To enable a comparative evaluation of the different ternary cement blends, two key environmental impact indicators were calculated: global warming potential (GWP) and energy consumption, as presented in Fig. 14(a) and (b). These indicators were normalized per 1 kg of ternary blend produced. To account for variability in sourcing and logistics, European

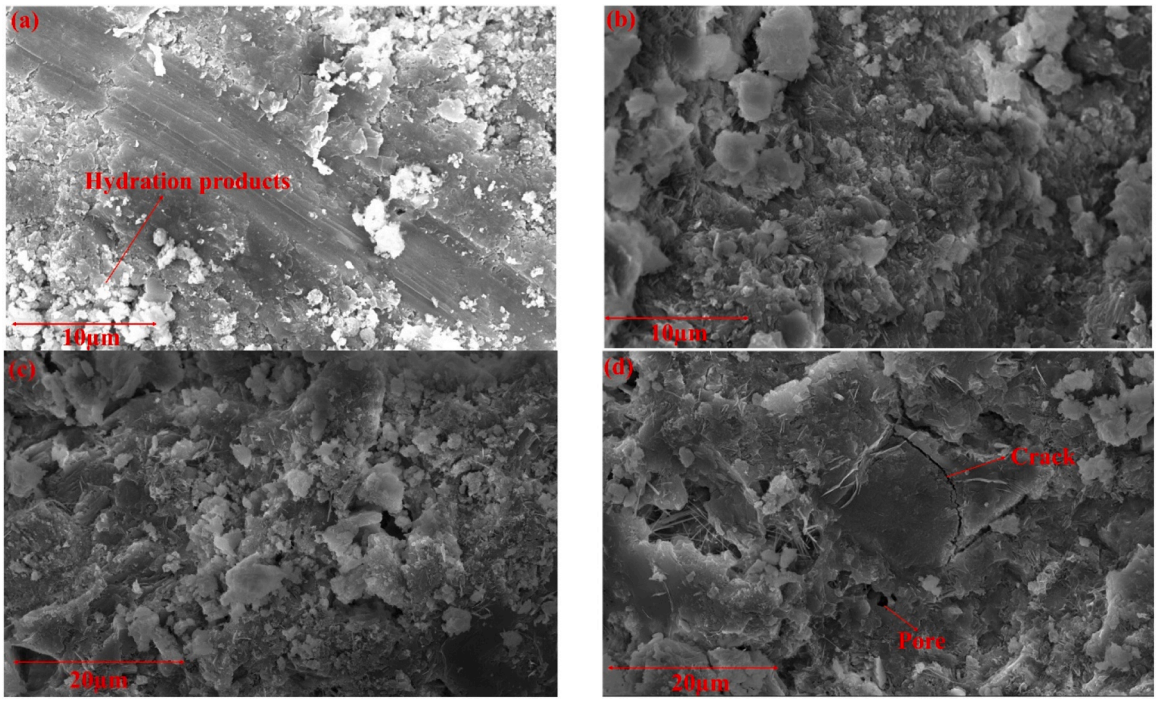

Fig. 13. SEM morphologies of hydration products of ternary blends at the age of 28 days. (a) CsCit; (b) Cs; (c) LsCit; (d) Ls.

Table 7
Leaching of inorganic contaminants measured by a one-stage batch leaching test.

Mixture	Leaching ions (mg/L)							pH
	Al	Cr	V	Fe	Na	K	Ca	
CsCit	0.390	0.012	bdl	0.019	75.734	195.454	657.508	12.81
CsHCit	0.389	0.015	bdl	0.011	74.123	227.341	634.839	12.66
Cs	0.408	0.010	bdl	0.014	76.301	173.708	506.471	12.78
LsCit	0.343	0.019	bdl	0.116	78.718	209.200	555.595	12.80
LsHCit	0.320	0.016	bdl	0.006	77.398	240.469	669.974	12.71
Ls	0.335	0.014	bdl	0.007	78.349	181.168	675.537	12.65

Note: bdl-below the detection limit.

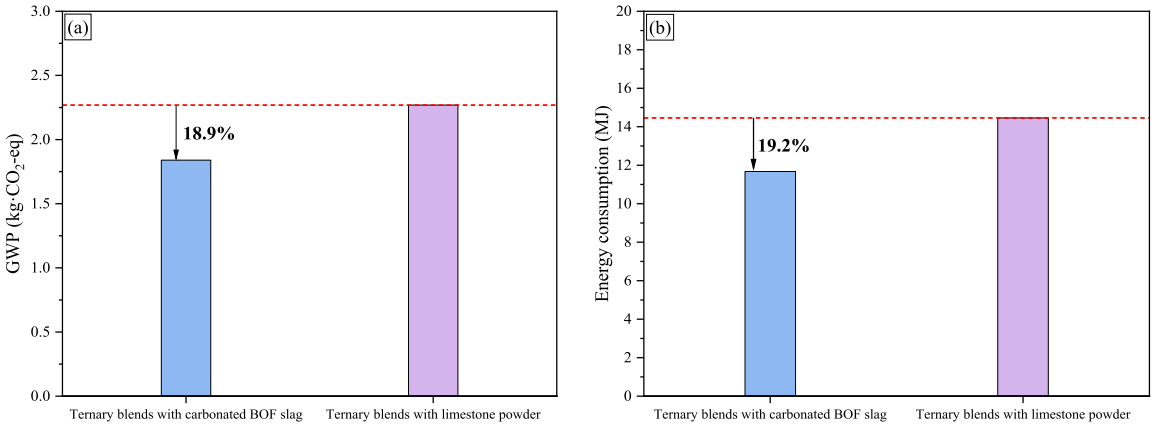

Fig. 14. The LCA of ternary blends: (a) The global warming potential (GWP); (b) The energy consumption.

average values were adopted to ensure consistency. GWP results were expressed in terms of kilograms of CO_2-equivalent (CO_2-eq), while energy consumption was quantified as cumulative energy demand (CED) in megajoules (MJ), following the methodology in [60]. The results indicate that the substitution of Ls with Cs reduced both CO_2 emissions and energy consumption. As shown in Fig. 14(a) and (b), the ternary blends incorporating Cs reduced 18.9% and 19.2% of CO_2 emissions and energy consumption, compared to those containing Ls. In terms of availability, the supply of fly ash is declining globally due to the phase-out of coal-fired power plants, while granulated blast furnace slag is geographically limited and largely allocated to the steel industry [61]. In contrast, BOF slag is an abundant byproduct of steelmaking, and its

carbonation treatment not only improves its reactivity but also provides permanent CO_2 sequestration [14]. Regarding embodied energy and CO_2 footprint, carbonation of BOF slag has been reported to achieve a negative net CO_2 balance, as the uptake of CO_2 during carbonation exceeds the emissions associated with grinding processing [62]. Notably, the reduction in CO_2 emissions is more substantial than that of energy consumption, underscoring the potential of Cs as a more sustainable alternative to conventional SCMs. However, when considering scalability, the energy consumption and CO_2 emissions generated by the carbonation process itself must be factored in. Industrial carbonation processes may require additional energy inputs for grinding, maintaining controlled CO_2 concentrations, or reactor operation, which could partially offset the environmental benefits observed at the laboratory scale [63]. On the other hand, large-scale carbonation processes can directly utilize industrial flue gas, reducing purification requirements while creating permanent CO_2 sinks [64]. Consequently, the net environmental benefit of Cs ultimately hinges on optimizing process parameters, maximizing CO_2 absorption while minimizing auxiliary energy consumption. This challenge demands urgent technical-economic and LCA studies.

In LCA, it is essential to evaluate the level of uncertainty, which often arises from data limitations, measurement inaccuracies, and assumptions embedded in the models, but it can be effectively mitigated through sensitivity analysis [65]. In this study, BOF slag and Ls were considered the primary variables in LC3 production, while the two admixtures were treated as secondary variables, with their prices partially affected by transportation costs. Given recent global fuel supply challenges that may impact LC3 costs, a sensitivity analysis was conducted to assess the effects of diesel prices and transportation distance on the costs of BOF slag, Ls, and the two admixtures. The transportation distance was assumed to range from 100 km to 1000 km, with 300 km increments, as shown in Table 8. Transport distance increases both GWP and CED, with CED being more sensitive. At all distances, Cs-based blends show lower GWP and CED than Ls-based blends. Cs is a byproduct, with all energy consumption attributed to the steel-making factory while LS requires additional mining. Both materials respond similarly to increased distance, but since Cs-based blends start at a lower baseline, their advantage is maintained even as transport distance grows. This indicates that transportation is not a decisive factor in choosing between Cs and Ls. Cs remains environmentally preferable in both indicators. Cs–based ternary blends consistently outperform Ls-based blends in terms of environmental impact.

Table 8
Sensitivity analysis of LC3.

Transport distance (km)	Ternary cement blends with Cs		Ternary cement blends with Ls	
	GWP (kg•CO_2-eq)	CED (MJ)	GWP (kg•CO_2-eq)	CED (MJ)
100	456.64	3042.73	469.81	3117.05
400	474.90	3300.86	488.28	3375.19
700	493.15	3558.92	506.76	3633.32
1000	511.40	3817.14	525.24	3891.46

4. Conclusions

In this study, carbonated Basic Oxygen Furnace (BOF) slag and calcined low-grade Dutch clay were combined into a cementitious system to develop ternary blend formulations, which were systematically compared with the conventional Limestone Calcined Clay Cement (LC3). Additionally, varying dosages of potassium citrate (citrate) were evaluated as an alternative admixture to the commonly used polycarboxylic acid-based superplasticizer (SP). Based on a comprehensive suite of experimental investigations, including mineralogical analysis, flowability, hydration behavior, mechanical performance, microstructural characterization, environmental impact assessment, and leaching behavior, the following key conclusions can be drawn:

1. Effect of Carbonated BOF Slag (Cs) replacement: Replacing limestone powder (Ls) with Cs in the ternary blends enhances hydration, as evidenced by higher cumulative heat release and increased chemically bound water. Despite the associated reduction in flowability and delayed hydration, the improved hydration contributes to higher compressive strength. Additionally, the incorporation of Cs enhances 28-day compressive strength by 23.9% and 29.7% relative to conventional LC3 systems using 0.1 wt.% citrate and SP.
2. Synergistic role of potassium citrate (citrate): Although hydration is slightly delayed, the presence of citrate results in increased overall hydration heat, leading to enhanced mechanical performance. Citrate demonstrates a dual function in the LC3 system, acting both as a water-reducing agent and an activator. Its activating effect is more pronounced in systems containing iron-rich by-products such as BOF slag, compared to systems incorporating limestone powder (Ls). The blend incorporating Ls and 0.1 wt.% citrate exhibited a 9.1% increase in flowability relative to the sample modified with SP alone. After 28 days of curing, the compressive strength of citrate-modified samples increased by 6.8% and 11.8% compared to their SP-modified counterparts.
3. Environmental impact reduction: Ternary blends incorporating Cs exhibit lower CO_2 emissions and energy consumption compared to those with Ls. Specifically, the energy consumption of blends with Cs is reduced by 19.2% relative to reference LC3. This demonstrates the strong potential of replacing Ls with Cs to reduce the environmental footprint of concrete production.

Future research should focus on evaluating the long-term durability of the LC3–Cs–citrate system under aggressive environments, including sulfate, chloride, and carbonation exposure, to validate its suitability for large-scale infrastructure. Further work is also needed on scaling the system for industrial use, assessing compatibility with commercial grinding, mixing, and curing processes, and analyzing variability in industrial Cs and low-grade clay sources. Additionally, exploring other organic admixtures with similar chelating or hydration-modifying capabilities may reveal synergistic effects or more efficient alternatives to citrate, enabling further optimization of workability, strength development, and sustainability performance.

CRediT authorship contribution statement

Zixing Liu: Methodology, Investigation, Data curation, Formal analysis, Validation, Writing – original draft. **Yanjie Tang:** Conceptualization, Methodology, Data curation, Writing – review & editing. **K. Schollbach:** Supervision, Project administration, Writing – review & editing. **H.J.H. Brouwers:** Funding acquisition, Supervision, Writing – review & editing.

Declaration of Competing Interest

The authors declare that they have no known competing financial interests or personal relationships that could have appeared to influence the work reported in this paper.

Acknowledgment

This research is supported by the China Scholarship Council (No.202106060060) and the Department of the Built Environment at Eindhoven University of Technology. The authors also gratefully acknowledge Heidelberg Materials for providing the cement, TCKI for the clays, and Tata Steel for the BOF slag.

Appendix A. Supporting information

Supplementary data associated with this article can be found in the online version at doi:10.1016/j.conbuildmat.2026.145232.

Data availability

Data will be made available on request.

References

[1] M. Sharma, S. Bishnoi, F. Martirena, K. Scrivener, Limestone calcined clay cement and concrete: a state-of-the-art review, Cem. Concr. Res (2021) 149, https://doi.org/10.1016/j.cemconres.2021.106564.

[2] P. Ramshankar, P. Ganeshan, K. Raja, B. NagarajaGanesh, Experimental investigation of the structural performance of concrete containing cellulose fibers and the anti-corrosive effect of green corrosion inhibitors, Civ. Environ. Eng. Rep. 34 (2024) 22–44, https://doi.org/10.59440/ceer/187189.

[3] M. Antoni, J. Rossen, F. Martirena, K. Scrivener, Cement substitution by a combination of metakaolin and limestone, Cem. Concr. Res 42 (2012) 1579–1589, https://doi.org/10.1016/j.cemconres.2012.09.006.

[4] K. Scrivener, F. Avet, H. Maraghechi, F. Zunino, J. Ston, W. Hanpongpun, et al., Impacting factors and properties of limestone calcined clay cements (LC3), Green. Mater. 7 (2018) 3–14, https://doi.org/10.1680/jgrma.18.00029.

[5] F. Avet, L. Sofia, K. Scrivener, Concrete performance of limestone calcined clay cement (LC3) compared with conventional cements, Adv. Civ. Eng. Mater. 8 (2019) 275–286, https://doi.org/10.1520/ACEM20190052.

[6] G. Cardinaud, E. Rozière, O. Martinage, A. Loukili, L. Barnes-Davin, M. Paris, et al., Calcined clay – Limestone cements: Hydration processes with high and low-grade kaolinite clays, Constr. Build. Mater. (2021) 277, https://doi.org/10.1016/j.conbuildmat.2021.122271.

[7] B. Kanagaraj, N. Anand, R. Samuvel Raj, E. Lubloy, Techno-socio-economic aspects of Portland cement, Geopolymer, and Limestone Calcined Clay Cement (LC3) composite systems: A-State-of-Art-Review, Constr. Build. Mater. 398 (2023) 132484, https://doi.org/10.1016/j.conbuildmat.2023.132484.

[8] K. Scrivener, F. Martirena, S. Bishnoi, S. Maity, Calcined clay limestone cements (LC3, Cem. Concr. Res 114 (2018) 49–56, https://doi.org/10.1016/j.cemconres.2017.08.017.

[9] F. Zunino, F. Martirena, K. Scrivener, Limestone calcined clay cements (lc3, Acids Mater. J. 118 (2021) 49–60, https://doi.org/10.14359/51730422.

[10] D. Zheng, X. Liang, H. Cui, W. Tang, W. Liu, D. Zhou, Study of performances and microstructures of mortar with calcined low-grade clay, Constr. Build. Mater. 327 (2022) 126963, https://doi.org/10.1016/j.conbuildmat.2022.126963.

[11] A. Dixit, H. Du, S.D. Pang, Performance of mortar incorporating calcined marine clays with varying kaolinite content, J. Clean. Prod. 282 (2021) 124513, https://doi.org/10.1016/j.jclepro.2020.124513.

[12] A.M. Kaja, K. Schollbach, S. Melzer, S.R. van der Laan, H.J.H. Brouwers, Q. Yu, Hydration of potassium citrate-activated BOF slag, Cem. Concr. Res 140 (2021) 106291, https://doi.org/10.1016/j.cemconres.2020.106291.

[13] K.R. Reddy, J.K. Chetri, G. Kumar, D.G. Grubb, Effect of basic oxygen furnace slag type on carbon dioxide sequestration from landfill gas emissions, Waste Manag. 85 (2019) 425–436, https://doi.org/10.1016/j.wasman.2019.01.013.

[14] G. Liu, Y. Tang, J. Wang, Effects of carbonation degree of semi-dry carbonated converter steel slag on the performance of blended cement mortar – reactivity, hydration, and strength, J. Build. Eng. 63 (2023) 105529, https://doi.org/10.1016/j.jobe.2022.105529.

[15] G. Liu, K. Schollbach, P. Li, H.J.H. Brouwers, Valorization of converter steel slag into eco-friendly ultra-high performance concrete by ambient CO2 pre-treatment, Constr. Build. Mater. (2021) 280, https://doi.org/10.1016/j.conbuildmat.2021.122580.

[16] W. Schwarz, Novel cement matrices by accelerated hydration of the ferrite phase in portland cement via chemical activation: kinetics and cementitious properties, Adv. Cem. Based Mater. 2 (1995) 189–200, https://doi.org/10.1016/1065-7355(95)90003-9.

[17] Q. Song, M.Z. Guo, L. Wang, T.C. Ling, Use of steel slag as sustainable construction materials: A review of accelerated carbonation treatment, Resour. Conserv Recycl 173 (2021) 105740, https://doi.org/10.1016/j.resconrec.2021.105740.

[18] G. Liu, R. Zhang, Z. Gu, J. Wang, Evaluation of calcined coal slime in binary and ternary ordinary portland cement composites: The role of calcination temperature, Constr. Build. Mater. 403 (2023) 133091, https://doi.org/10.1016/j.conbuildmat.2023.133091.

[19] Z. Shi, S. Ferreiro, B. Lothenbach, M.R. Geiker, W. Kunther, J. Kaufmann, et al., Sulfate resistance of calcined clay – Limestone – Portland cements, Cem. Concr. Res 116 (2019) 238–251, https://doi.org/10.1016/j.cemconres.2018.11.003.

[20] G. Liu, J. Wang, Utilization of carbonated alkaline solid wastes in ordinary Portland cement-metakaolin-limestone ternary mixture: Underlying the role of low grade-sustainable calcium carbonate sources, J. Clean. Prod. (2024) 456, https://doi.org/10.1016/j.jclepro.2024.142382.

[21] A. Zolfagharnasab, A.A. Ramezanianpour, F. Bahman-Zadeh, Investigating the potential of low-grade calcined clays to produce durable LC3 binders against chloride ions attack, Constr. Build. Mater. (2021) 303, https://doi.org/10.1016/j.conbuildmat.2021.124541.

[22] K.D. Musbau, J.T. Kolawole, A.J. Babafemi, O.B. Olalusi, Comparative performance of limestone calcined clay and limestone calcined laterite blended cement concrete, Clean. Eng. Technol. (2021) 4, https://doi.org/10.1016/j.clet.2021.100264.

[23] R. Fernandez, F. Martirena, K.L. Scrivener, The origin of the pozzolanic activity of calcined clay minerals: A comparison between kaolinite, illite and montmorillonite, Cem. Concr. Res 41 (2011) 113–122, https://doi.org/10.1016/j.cemconres.2010.09.013.

[24] F. Martirena, R. Almenares, F. Zunino, A. Alujas, K. Scrivener, Color control in industrial clay calcination, RILEM Tech. Lett. 5 (2020) 1–7, https://doi.org/10.21809/RILEMTECHLETT.2020.107.

[25] BS EN196-1. Methods of testing cement Part 1 Determination of strength. British Standard 2005;3.

[26] A.C.A. Muller, K.L. Scrivener, A reassessment of mercury intrusion porosimetry by comparison with ^{1}H NMR relaxometry, Cem. Concr. Res 100 (2017) 350–360, https://doi.org/10.1016/j.cemconres.2017.05.024.

[27] Z. Zhang, Y. Zhu, H. Zhu, Y. Zhang, J.L. Provis, H. Wang, Effect of drying procedures on pore structure and phase evolution of alkali-activated cements, Cem. Concr. Compos 96 (2019) 194–203, https://doi.org/10.1016/j.cemconcomp.2018.12.003.

[28] G. Liu, Y. Tang, J. Wang, Recycling and valorization of hydrated cement blends in mortars via semi-dry carbonation – The role of waste glass, granulated blast furnace slag and fly ash, Constr. Build. Mater. (2023) 401, https://doi.org/10.1016/j.conbuildmat.2023.132987.

[29] G. Bayon, N. Freslon, Y. Germain, I.N. Bindeman, A. Trinquier, J.A. Barrat, A global survey of radiogenic strontium isotopes in river sediments, Chem. Geol. 559 (2021) 119958, https://doi.org/10.1016/j.chemgeo.2020.119958.

[30] M. Guo, G. Gong, Y. Yue, F. Xing, Y. Zhou, B. Hu, Performance evaluation of recycled aggregate concrete incorporating limestone calcined clay cement (LC3), J. Clean. Prod. (2022) 366, https://doi.org/10.1016/j.jclepro.2022.132820.

[31] R.G. Pillai, R. Gettu, M. Santhanam, S. Rengaraju, Y. Dhandapani, S. Rathnarajan, et al., Service life and life cycle assessment of reinforced concrete systems with limestone calcined clay cement (LC3), Cem. Concr. Res 118 (2019) 111–119, https://doi.org/10.1016/j.cemconres.2018.11.019.

[32] D. Zhou, R. Wang, M. Tyrer, H. Wong, C. Cheeseman, Sustainable infrastructure development through use of calcined excavated waste clay as a supplementary cementitious material, J. Clean. Prod. 168 (2017) 1180–1192, https://doi.org/10.1016/j.jclepro.2017.09.098.

[33] M. Tahmasebi Yamchelou, D. Law, R. Brkljača, C. Gunasekara, J. Li, I. Patnaikuni, Geopolymer synthesis using low-grade clays, Constr. Build. Mater. (2021) 268, https://doi.org/10.1016/j.conbuildmat.2020.121066.

[34] X. Zhou, K. Zheng, L. Chen, G. Prateek, Q. Yuan, An approach to improve the reactivity of basic oxygen furnace slag: Accelerated carbonation and the combined use of metakaolin, Constr. Build. Mater. 379 (2023) 131218, https://doi.org/10.1016/j.conbuildmat.2023.131218.

[35] R.S. Lin, S. Oh, W. Du, X.Y. Wang, Strengthening the performance of limestone-calcined clay cement (LC3) using nano silica, Constr. Build. Mater. 340 (2022) 127723, https://doi.org/10.1016/j.conbuildmat.2022.127723.

[36] R.S. Lin, H.S. Lee, Y. Han, X.Y. Wang, Experimental studies on hydration–strength–durability of limestone-cement-calcined Hwangtoh clay ternary composite, Constr. Build. Mater. (2021) 269, https://doi.org/10.1016/j.conbuildmat.2020.121290.

[37] D. Wang, C. Shi, N. Farzadnia, Z. Shi, H. Jia, Z. Ou, A review on use of limestone powder in cement-based materials: Mechanism, hydration and microstructures, Constr. Build. Mater. 181 (2018) 659–672, https://doi.org/10.1016/j.conbuildmat.2018.06.075.

[38] P. Pichniarczyk, T. Baran, Influence of lead and vanadium on the setting of Portland cement CEM I 52,5N SR3/NA, J. Therm. Anal. Calor. 131 (2018) 2321–2328, https://doi.org/10.1007/s10973-017-6762-x.

[39] Y. Tang, G. Liu, K. Schollbach, Y. Chen, W. Chen, H.J.H. Brouwers, Re-cementation effects by carbonation and the pozzolanic reaction on LWAs produced by hydrated cement paste powder, J. Clean. Prod. 377 (2022) 134529, https://doi.org/10.1016/j.jclepro.2022.134529.

[40] G. Le Saoût, V. Kocaba, K. Scrivener, Application of the Rietveld method to the analysis of anhydrous cement, Cem. Concr. Res 41 (2011) 133–148, https://doi.org/10.1016/j.cemconres.2010.10.003.

[41] K. Rozov, U. Berner, C. Taviot-Gueho, F. Leroux, G. Renaudin, D. Kulik, et al., Synthesis and characterization of the LDH hydrotalcite-pyroaurite solid-solution series, Cem. Concr. Res 40 (2010) 1248–1254, https://doi.org/10.1016/j.cemconres.2009.08.031.

[42] Y. Briki, M. Zajac, M.Ben Haha, K. Scrivener, Impact of limestone fineness on cement hydration at early age, Cem. Concr. Res (2021) 147, https://doi.org/10.1016/j.cemconres.2021.106515.

[43] L. Wang, N. Ur Rehman, I. Curosu, Z. Zhu, M.A.B. Beigh, M. Liebscher, et al., On the use of limestone calcined clay cement (LC3) in high-strength strain-hardening cement-based composites (HS-SHCC), Cem. Concr. Res 144 (2021) 106421, https://doi.org/10.1016/j.cemconres.2021.106421.

[44] S. Adu-Amankwah, M. Zajac, J. Skoček, J. Němeček, M.Ben Haha, L. Black, Combined influence of carbonation and leaching on freeze-thaw resistance of limestone ternary cement concrete, Constr. Build. Mater. (2021) 307, https://doi.org/10.1016/j.conbuildmat.2021.125087.

[45] Q. Huang, Z. Tao, Z. Pan, R. Wuhrer, M. Rahme, Use of sodium/potassium citrate to enhance strength development in carbonate-activated hybrid cement, Constr. Build. Mater. 350 (2022) 128913, https://doi.org/10.1016/j.conbuildmat.2022.128913.

[46] Z.N. Kadhim, A.K. Ibraheem, M.J. Al-Assadi, Effect of Citrate Salts of Li+, Na+ and K+ on Some Physical Properties of Ordinary Portland Cement (OPC), J. Mater. Appl. Sci. 1 (2017) 1–8.
[47] S. Alahrache, F. Winnefeld, J.B. Champenois, F. Hesselbarth, B. Lothenbach, Chemical activation of hybrid binders based on siliceous fly ash and Portland cement, Cem. Concr. Compos 66 (2016) 10–23, https://doi.org/10.1016/j.cemconcomp.2015.11.003.
[48] Y. Liu, T.C. Ling, M. Wang, Y.Y. Wu, Synergic performance of low-kaolinite calcined coal gangue blended with limestone in cement mortars, Constr. Build. Mater. 300 (2021) 124012, https://doi.org/10.1016/j.conbuildmat.2021.124012.
[49] F. Avet, K. Scrivener, Investigation of the calcined kaolinite content on the hydration of Limestone Calcined Clay Cement (LC3), Cem. Concr. Res 107 (2018) 124–135, https://doi.org/10.1016/j.cemconres.2018.02.016.
[50] H. Maraghechi, F. Avet, H. Wong, H. Kamyab, K. Scrivener, Performance of Limestone Calcined Clay Cement (LC3) with various kaolinite contents with respect to chloride transport, Mater. Struct. /Mater. Et. Constr. 51 (2018) 1–17, https://doi.org/10.1617/s11527-018-1255-3.
[51] V. Shah, A. Parashar, G. Mishra, S. Medepalli, S. Krishnan, S. Bishnoi, Influence of cement replacement by limestone calcined clay pozzolan on the engineering properties of mortar and concrete, Adv. Cem. Res. 32 (2020) 101–111, https://doi.org/10.1680/jadcr.18.00073.
[52] F. Bahman-Zadeh, A.A. Ramezanianpour, A. Zolfagharnasab, Effect of carbonation on chloride binding capacity of limestone calcined clay cement (LC3) and binary pastes, J. Build. Eng. 52 (2022) 104447, https://doi.org/10.1016/j.jobe.2022.104447.
[53] N. Blouch, K. Rashid, M. Ju, Exploring low-grade clay minerals diving into limestone calcined clay cement (LC3): Characterization – Hydration – Performance, J. Clean. Prod. 426 (2023) 139065, https://doi.org/10.1016/j.jclepro.2023.139065.
[54] C. Zhang, X. Kong, Z. Lu, D. Jansen, J. Pakusch, S. Wang, Pore structure of hardened cement paste containing colloidal polymers with varied glass transition temperature and surface charges, Cem. Concr. Compos 95 (2019) 154–168, https://doi.org/10.1016/j.cemconcomp.2018.11.001.
[55] X. Li, A. Wanner, C. Hesse, S. Friesen, J. Dengler, Clinker-free cement based on calcined clay, slag, portlandite, anhydrite, and C-S-H seeding: An SCM-based low-carbon cementitious binder approach, Constr. Build. Mater. (2024) 442, https://doi.org/10.1016/j.conbuildmat.2024.137546.
[56] M.J. Ahmed, K. Schollbach, S. van der Laan, H.J.H. Brouwers, Reactivity of air granulated basic oxygen furnace steel slag and its immobilization of heavy metals, J. Build. Eng. (2024) 91, https://doi.org/10.1016/j.jobe.2024.109704.
[57] A. Vollpracht, W. Brameshuber, Binding and leaching of trace elements in Portland cement pastes, Cem. Concr. Res 79 (2016) 76–92, https://doi.org/10.1016/j.cemconres.2015.08.002.
[58] G.M. Kim, J.G. Jang, F. Naeem, H.K. Lee, Heavy metal leaching, CO2 uptake and mechanical characteristics of carbonated porous concrete with alkali-activated slag and bottom ash, Int J. Concr. Struct. Mater. 9 (2015) 283–294, https://doi.org/10.1007/s40069-015-0111-x.
[59] T. Van Gerven, G. Cornelis, E. Vandoren, C. Vandecasteele, Effects of carbonation and leaching on porosity in cement-bound waste, Waste Manag. 27 (2007) 977–985, https://doi.org/10.1016/j.wasman.2006.05.008.
[60] T. Ding, J. Xiao, V.W.Y. Tam, A closed-loop life cycle assessment of recycled aggregate concrete utilization in China, Waste Manag. 56 (2016) 367–375, https://doi.org/10.1016/j.wasman.2016.05.031.
[61] K.L. Scrivener, V.M. John, E.M. Gartner, Eco-efficient cements: Potential economically viable solutions for a low-CO2 cement-based materials industry, Cem. Concr. Res 114 (2018) 2–26, https://doi.org/10.1016/j.cemconres.2018.03.015.
[62] R.M. Santos, J. Van Bouwel, E. Vandevelde, G. Mertens, J. Elsen, T. Van Gerven, Accelerated mineral carbonation of stainless steel slags for CO2 storage and waste valorization: Effect of process parameters on geochemical properties, Int. J. Greenh. Gas. Control 17 (2013) 32–45, https://doi.org/10.1016/j.ijggc.2013.04.004.
[63] G. Costa, A. Polettini, R. Pomi, A. Stramazzo, D. Zingaretti, Energetic assessment of CO2 sequestration through slurry carbonation of steel slag: a factorial study, Greenhouse Gases Science Technology 7 (2017) 530–541, https://doi.org/10.1002/ghg.1659.
[64] Li-Shan Xiao RWP-CCS-YPQ-HGEEC. Comparative Life Cycle Assessment (LCA) of Accelerated Carbonation Processes Using Steelmaking Slag for CO2 Fixation. Aerosol Air Qual Res 2014.
[65] L. Li, Y. Jiang, S.Y. Pan, T.C. Ling, Comparative life cycle assessment to maximize CO2 sequestration of steel slag products, Constr. Build. Mater. (2021) 298, https://doi.org/10.1016/j.conbuildmat.2021.123876.